

Generalized size scaling of metabolic rates based on single-cell measurements with freshwater phytoplankton

Silvia Zaoli^a, Andrea Giometto^b, Emilio Mara^ñon^c, St  phane Escrig^d, Anders Meibom^d, Arti Ahluwalia^{e,f}, Roman Stocker^g, Amos Maritan^h, and Andrea Rinaldo^{a,i,1}

^aLaboratory of Ecohydrology, Institute of Environmental Engineering,   cole Polytechnique F  d  rale de Lausanne, CH-1015 Lausanne, Switzerland; ^bDepartment of Physics, Harvard University, Cambridge, MA 02138; ^cDepartment of Ecology and Animal Biology, Universidad de Vigo, 36210 Vigo, Spain; ^dLaboratory of Biological Geochemistry, Institute of Environmental Engineering,   cole Polytechnique F  d  rale de Lausanne, CH-1015 Lausanne, Switzerland; ^eCentro di Ricerca "E. Piaggio," Universit   di Pisa, 56126 Pisa, Italy; ^fDepartment of Information Engineering, Universit   di Pisa, 56126 Pisa, Italy; ^gThe Environmental Microfluidics Laboratory, Department of Environmental Sciences, Eidgen  ssische Technische Hochschule Z  rich, 8092 Z  rich, Switzerland; ^hDepartment of Physics and Astronomy, Istituto Nazionale di Fisica Nucleare, 35131 Padova, Italy; and ⁱDipartimento di Ingegneria Civile, Edile e Ambientale, Universit   di Padova, I-35131 Padova, Italy

Contributed by Andrea Rinaldo, July 1, 2019 (sent for review April 30, 2019; reviewed by Paul G. Falkowski and Pablo A. Marquet)

Kleiber's law describes the scaling of metabolic rate with body size across several orders of magnitude in size and across taxa and is widely regarded as a fundamental law in biology. The physiological origins of Kleiber's law are still debated and generalizations of the law accounting for deviations from the scaling behavior have been proposed. Most theoretical and experimental studies of Kleiber's law, however, have focused on the relationship between the average body size of a species and its mean metabolic rate, neglecting intraspecific variation of these 2 traits. Here, we propose a theoretical characterization of such variation and report on proof-of-concept experiments with freshwater phytoplankton supporting such framework. We performed joint measurements at the single-cell level of cell volume and nitrogen/carbon uptake rates, as proxies of metabolic rates, of 3 phytoplankton species using nanoscale secondary ion mass spectrometry (NanoSIMS) and stable isotope labeling. Common scaling features of the distribution of nutrient uptake rates and cell volume are found to hold across 3 orders of magnitude in cell size. Once individual measurements of cell volume and nutrient uptake rate within a species are appropriately rescaled by a function of the average cell volume within each species, we find that intraspecific distributions of cell volume and metabolic rates collapse onto a universal curve. Based on the experimental results, this work provides the building blocks for a generalized form of Kleiber's law incorporating intraspecific, correlated variations of nutrient-uptake rates and body sizes.

phenotypic heterogeneity | *Synechococcus* | *Scenedesmus* | *Cryptomonas* | metabolic theory of ecology

Research across diverse systems has revealed remarkable regularities in the distributions of species, their abundances, and metabolic requirements (1–4), providing a foundation to predict how ecological communities assemble and respond to environmental change. Kleiber's law (1) is widely regarded as one of the most important of these regularities. It states that, across many orders of magnitude, the average metabolic rate B of an ensemble of organisms of a species scales with its average body mass, M , according to the power law $B = cM^\alpha$ (where α is a scaling exponent and c is a constant that may vary across different branches of the tree of life). The metabolic requirements of organisms underlie many fundamental biological properties, including life-history, population, and community attributes (5), giving Kleiber's law a central role in the understanding of ecosystem-level consequences of resource utilization (4, 6, 7). The majority of experimental studies support the claim that the exponent in Kleiber's law is $\alpha \simeq 3/4$ (8–10) and theoretical explanations that return this value have been proposed, based on general features of metabolic networks (11, 12). However,

the applicability of the law across taxa (13) and the universality of the exponent $3/4$ have been repeatedly challenged (14–18). Recent investigations point at corrections to the simple power-law scaling, which, however, proves a reasonable approximation across a wide range of body sizes (19, 20).

Most studies investigating Kleiber's law have measured average metabolic rates and body masses within individual species, so that each species is described by one point in (M, B) plots. However, these physiological traits are typically very heterogeneous within a population (14, 21), due to environmental fluctuations, to differences in life stages and physiological conditions, and to phenotypic heterogeneity, caused by either phenotypic plasticity or genetic differences. Such heterogeneity may be particularly important in natural settings, where it is increasingly being recognized as nature's solution to 2 challenges: resource limitation and fluctuations of the environment (22, 23). From an evolutionary point of view, body size and metabolic rate are heritable traits (24, 25), and quantifying their intraspecific variation is key to understanding how fast they evolve.

Community effects of variability in individual traits, including size and metabolic rates, have been predicted theoretically (22). Experimentally, the variability of metabolic rates among

Significance

Empirical laws predicting metabolic rates of a species by its average body mass neglect intraspecies variability arising from the range of physiologically feasible rates and phenotypic heterogeneity. We describe an exploratory experimental test of a theory that explicitly accounts for such variations. We show, by single-cell joint measurements of mass and uptake rates, how marginal distributions of mass and rates collapse onto a common master distribution for species spanning 3 orders of magnitude in cell volume. These results demonstrate the potential of a generalized scaling theory that goes beyond population averages to incorporate within-species variation.

Author contributions: A. Maritan and A.R. designed research; S.Z., A.G., E.M., and A. Meibom performed research; S.Z., E.M., S.E., A. Meibom, and R.S. contributed new reagents/analytic tools; S.Z., A.G., E.M., S.E., A.A., R.S., A. Maritan, and A.R. analyzed data; and S.Z., A.G., E.M., A.A., R.S., A. Maritan, and A.R. wrote the paper.

Reviewers: P.G.F., Rutgers University; and P.A.M., Pontificia Universidad del Chile.

The authors declare no conflict of interest.

This open access article is distributed under Creative Commons Attribution-NonCommercial-NoDerivatives License 4.0 (CC BY-NC-ND).

¹To whom correspondence may be addressed. Email: andrea.rinaldo@epfl.ch.

This article contains supporting information online at www.pnas.org/lookup/suppl/doi:10.1073/pnas.1906762116/-DCSupplemental.

Published online August 13, 2019.

individuals has been examined within single species or classes (14, 23, 26–28), often looking at species-specific molecular pathways as well as temporal fluctuations of individual rates (29). However, no systematic measurements of common patterns of intra- and interspecific metabolic rate heterogeneity and their covariation with body size seem to have been performed to date across a significant range of body sizes. Here, we aim at characterizing how the variability of body sizes and of metabolic rates within a species affects Kleiber's law and whether one can formulate a more general law that takes the intraspecific heterogeneity of physiological traits explicitly into account. At the community level, the metabolic theory of ecology can be used to link individual metabolism to the global carbon cycle (5, 30). The characterization of intraspecific variability of carbon uptake rates is a prerequisite for understanding how it affects the global carbon cycle—an interesting and timely avenue for future research.

Results

Previous work (31) has shown that intraspecific body size distributions of microorganisms display universal features such that the average body volume V of a species is sufficient to completely characterize such distributions. In mathematical terms, the intraspecific body size distribution $p_i(v)$ of species i can be expressed as $p_i(v) = p(v|V_i)$, where V_i is the average/characteristic body volume of species i , the expression “ $|V_i$ ” indicates conditioning on V_i , and the probability distribution p does not depend on other species-specific traits. Kleiber's law tells us that, at the species level, body size is a good predictor of metabolic rate. Therefore, we expect that, at the intraspecific level, a part of the metabolic rate variability will be explained by the body size variability and therefore inherit the universal features of intraspecific body size distributions. However, additional variability may emerge due to other physiological heterogeneity among individuals. This additional component of the variability might also display universal features, as suggested by the study of temporal metabolic rate fluctuations by Labra et al. (29). Based on this evidence, we hypothesize that the intraspecific metabolic rate distribution $p_i(b)$, where b is the metabolic rate of individuals of species i , can be expressed as $p(b|V_i)$ similarly to the intraspecific body size distribution, where the probability distribution p again does not depend on other species-specific traits. Under this hypothesis, knowing the functional dependence of $p(b|V)$ on b and V would allow us to compute the intraspecific metabolic rate distribution for any species based solely on its mean body volume V . The existence of such a universal distribution of metabolic rates implies that their typical range of variation within a species scales with V (SI Appendix). Existing data pose a constraint on the functional form of $p(b|V)$, given that it must produce Kleiber's law, $B \propto V^\alpha$, when the average metabolic rate B is computed from $p(b|V)$ as $B = \int b p(b|V) db$. Identifying the functional form of $p(b|V)$ compatible with experimental data would provide a first generalization of Kleiber's law, accounting for the variability of b regardless of v within a species. A further generalization of Kleiber's law would be provided by the joint distribution $p(v, b|V)$ (Materials and Methods), which encapsulates the covariation of v and b , and of which $p(v|V)$ and $p(b|V)$ are the marginal distributions; i.e., $p(v|V) = \int p(v, b|V) db$ and $p(b|V) = \int p(v, b|V) dv$.

Our experiments are aimed at demonstrating the universality of the intraspecific variability of v and b . Reconstructing the joint distribution $p(v, b|V)$ empirically requires simultaneous measurements of metabolic rates b and body volumes v of individuals of different species with different mean volumes V . Verifying the universality of such distribution, however, requires a sufficiently smooth reconstruction of $p(v, b|V)$, which we cannot achieve with available experimental approaches because of the relatively small number of individuals that we can probe for each species.

Furthermore, to address questions concerning the universality of $p(v, b|V)$, one needs to measure individual body sizes and metabolic rates of species with average size spanning a broad range, ideally a few orders of magnitude, with the same experimental procedure. Due to these severe requirements, we are capable of estimating only the marginal distributions $p(v|V)$ and $p(b|V)$, which is less data demanding, and testing their universality. Our measurements of $p(v|V)$ agree with previous results (31) and support the scaling form

$$p(v|V) = \frac{1}{v} F\left(\frac{v}{V}\right), \quad [1]$$

where the function F is species independent. Here, we hypothesize and test the validity of the scaling form for the intraspecific distribution of metabolic rates,

$$p(b|V) = \frac{1}{b} G\left(\frac{b}{V^\alpha}\right) \quad [2]$$

(with $\alpha > 0$), where G is again a species-independent function (see SI Appendix for the properties that F and G must satisfy). This hypothesis can be shown to imply the canonical form of Kleiber's law with exponent α for the mean metabolic rate B and the mean volume V (i.e., $B \propto V^\alpha$). Note that an equation similar to Eq. 2 has been proposed previously (14) and shown to be compatible with experimental data on metabolic rate fluctuations for small mammals. We discuss the relationship between Eq. 2 of this work and equation 2 of ref. 14 in Materials and Methods. In our experiments, we measured 2 nutrient uptake rates (b_C and b_N), one for carbon (subscript C) and one for nitrogen (subscript N), as proxies of the metabolic rate (32). We hypothesize that both satisfy Eq. 2 with 2 different exponents (α_C and α_N) and 2 different scaling functions (G_C and G_N).

To test this hypothesis, we measured experimentally nutrient uptake rates and cell volumes of individual freshwater phytoplankton cells of the 3 species *Synechococcus* sp., *Scenedesmus obliquus*, and *Cryptomonas ovata*, together covering 3 orders of magnitude in cell volume ($1 \mu\text{m}^3$ to $10^3 \mu\text{m}^3$). We chose to perform experiments with freshwater phytoplankton because they cover a significant size range while maintaining functional similarity and allowing uniform measurement techniques and because of their ecological relevance as primary producers at the heart of marine and freshwater trophic webs (17). We used nanoscale secondary ion mass spectrometry (NanoSIMS) (Materials and Methods) in combination with stable isotope labeling to simultaneously measure cell size and rates of nutrient (carbon and nitrogen) uptake—the latter a measure of metabolic rate of particular relevance for phytoplanktonic communities—although aware of the difficulties of constraining measures of heat production and photosynthetic energy conversion in nature and in cultures (33, 34). Specifically, we targeted nitrogen and carbon uptake because phytoplankton photosynthesis has been routinely measured via C uptake for decades (16, 32) and because C and N uptakes tend to be coupled during photoautotrophic exponential growth (7, 35). The cell size was measured as the volume v of individual cells, rather than their mass, based on density being nearly constant within species. Monocultures of the 3 study species were exposed to a medium enriched in 2 rare isotopes of carbon and nitrogen, ^{13}C and ^{15}N , for a known amount of time (Materials and Methods). By measuring the uptakes of ^{13}C and ^{15}N of a cell, and knowing the isotope ratios in the medium, we can compute its total carbon and nitrogen uptake and therefore the uptake rates b_C and b_N . The uptakes were obtained as follows. Each individual cell's ^{13}C :C and ^{15}N :N ratios were measured by NanoSIMS imaging (Materials and Methods and Fig. 1). The total cell content of ^{13}C and ^{15}N was then obtained by multiplying such ratios by the total cell content of C and N, inferred from the species averages measured by

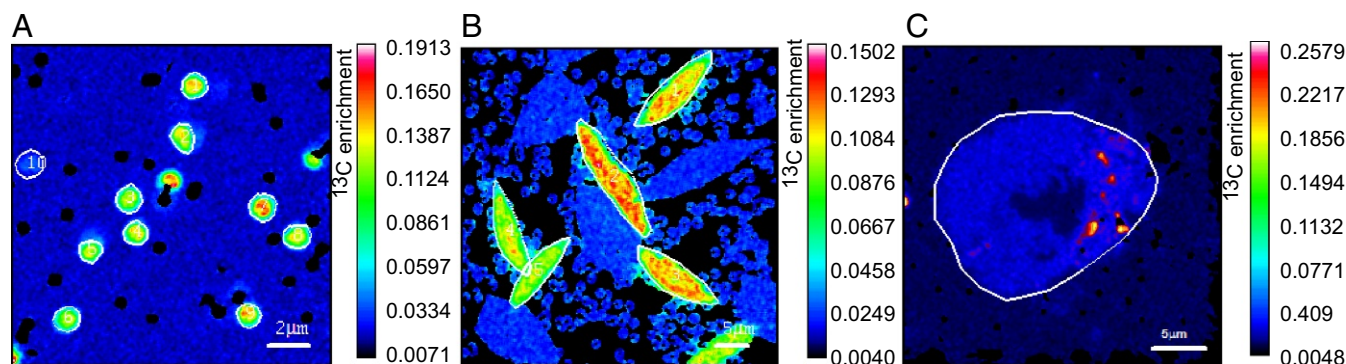


Fig. 1. Examples of ratio images from NanoSIMS experiments. Colors (see color bars) represent ^{13}C enrichment (relative to the control sample), measured by the ratio $(r_{\text{mes}} - r_{\text{control}})/r_{\text{control}} \times 1,000$, where $r = {}^{13}\text{C}/{}^{12}\text{C}$ and the subscripts mes and control indicate the isotope ratios measured in the ^{13}C -enriched and the control samples, respectively. White contours highlight the ROI over which the isotopic ratio is averaged. (A) *Synechococcus* sp. (B) *S. obliquus*. (C) *C. ovata*.

gas chromatography (*SI Appendix*) as explained in *Materials and Methods*. The uptake was then obtained by subtracting the natural content of ^{13}C and ^{15}N , known from the control samples. The volume v of each cell was also inferred from the NanoSIMS image processing.

The experiments thus provide a dataset of N joint measurements of single-cell uptake rates b_C , b_N and cell volumes v , which are shown in Fig. 2 *A* and *B*, for each of the 3 phytoplankton species employed here. Each point represents a single cell and the species averages V , B_C , B_N are highlighted. It can be seen that average uptake rates scale with the species' average cell volume, with exponents $\alpha_C = 0.69 \pm 0.01$ for carbon and $\alpha_N = 0.56 \pm 0.01$ for nitrogen, where the exponents have been obtained by linear least-squares fitting of log-transformed data. The fact that these values are close to $2/3$, which is the exponent for the scaling of the cell surface area as a function of the cell volume, may suggest that uptake is limited by membrane transport, an observation consistent with the high nutrient concentration used in the experiments (but see also the discussion concerning low-irradiance experimental conditions). At the intraspecific level, the correlation of B and V visible in Fig. 2 *A* and *B* is based on the assumption that the interspecific scaling of carbon and nitrogen content holds also at the intraspecific level (*Materials and Methods, Computation of Size and Uptake Rates*), an assumption which could not be verified experimentally due to the impossibility of measuring absolute C and N levels in cells to the accuracy required with the available experimental methods. On the other hand, unit carbon and nitrogen uptake rates $\tilde{b}_i = b_i/c_i$ (c_C is the total cell content of carbon and c_N is the total cell content of nitrogen), shown in Fig. 2 *C* and *D*, are not affected by this assumption. Within each species, the correlations of unit carbon and nitrogen uptake rates with cell volume are weak, implying that the variabilities of cell size and unit uptake rates for cells of the same species are approximately independent. The correlations of total uptake rates b_C and b_N with cell volume V are therefore mediated by the cellular content of carbon and nitrogen. A small number of outliers among the *Synechococcus* cells, possibly affected by errors during manipulation or NanoSIMS analysis, were excluded from the analysis (*SI Appendix*). Carbon-specific and nitrogen-specific uptake rates show a strong positive correlation (Pearson coefficient 0.83, Fig. 2*E*). Note that we consider nutrient-specific rates to assess the existence of correlations because the multiplication by cell volume (which is necessary to obtain total uptake rates) introduces a strong spurious effect.

The marginal distributions $p(v|V)$, $p(b_C|V)$, and $p(b_N|V)$ were obtained by binning data and are shown in Figs. 3*A* and 4*A* and *C*, respectively. The validity of the scaling forms in Eqs.

1 and 2 can be tested via data collapse as follows. If Eq. 1 is verified, plotting the quantity v/V vs. $v \cdot p(v|V)$ should cause curves from different species to collapse onto the same universal curve, which provides the plot of the scaling function F . Similarly, if Eq. 2 holds, the curves obtained by plotting b/V^α vs. $b \cdot p(b|V)$ should collapse on the function G , which can in principle be different for carbon and nitrogen uptake. Such collapses are shown in Fig. 3*B* for $p(v|V)$ and in Fig. 4*B* and *D* for $p(b_C|V)$ and $p(b_N|V)$, respectively; thus Eqs. 1 and 2 hold true. We estimated the exponents α_C and α_N by computing the values that give the best collapses of $p(b_C|V)$ and $p(b_N|V)$ for the 3 species, using the method described in ref. 36, yielding $\alpha_C = 0.685 \pm 0.002$ and $\alpha_N = 0.585 \pm 0.005$. The error is computed as the value of the exponent at which the error functional P_b (defined in ref. 36 by the sum of the areas enclosed between all pairs of rescaled curves) is 1% larger than its value at the minimum (*SI Appendix*). Note that by fixing the threshold for the acceptance of the collapse at 10%, the error becomes ± 0.01 . It should also be noted that we had estimated these exponents previously via linear least-squares fitting of log-transformed data, and the 2 methods of estimation give compatible values for each exponent. Forcing scaling exponents equal to $2/3$ or $3/4$ irrespective of C, N significantly worsened the collapse (*SI Appendix*). Furthermore, if Eq. 2 holds true, the probability distribution for the variable $Y = \log(b/V^\alpha)$ is simply $p(Y) = G(e^Y)$, regardless of the species. By rescaling the data in this way, we can use the k-sample Anderson–Darling test to determine whether the null hypothesis—namely that the rescaled samples from the 3 species are drawn from the same distribution—is rejected. This gives us a statistical procedure to test whether our hypothesis is consistent with the data. Analogous considerations hold for Eq. 1, where the rescaled variable used for the statistical testing is $X = \log(v/V)$. For the intraspecific body size distributions, the k-sample Anderson–Darling test on the 3 rescaled samples does not reject the hypothesis that the samples come from the same distribution at the 5% confidence level (P value = 0.17), supporting the hypothesis that cell size distributions have the scaling form given by Eq. 1.

Similarly, for both carbon and nitrogen uptake rates, the k-sample Anderson–Darling tests on the rescaled samples (*Materials and Methods*) do not reject the hypothesis that the 3 samples come from the same distribution at the 5% confidence level (with P values of 0.09 and 0.07, respectively), supporting the rescaling framework hypothesized in Eq. 2. We note that when testing for the universality of scaling probability distributions, we find it remarkable that the statistical test does not rule out the null hypothesis. In fact, any small correction (e.g., logarithmic) to the

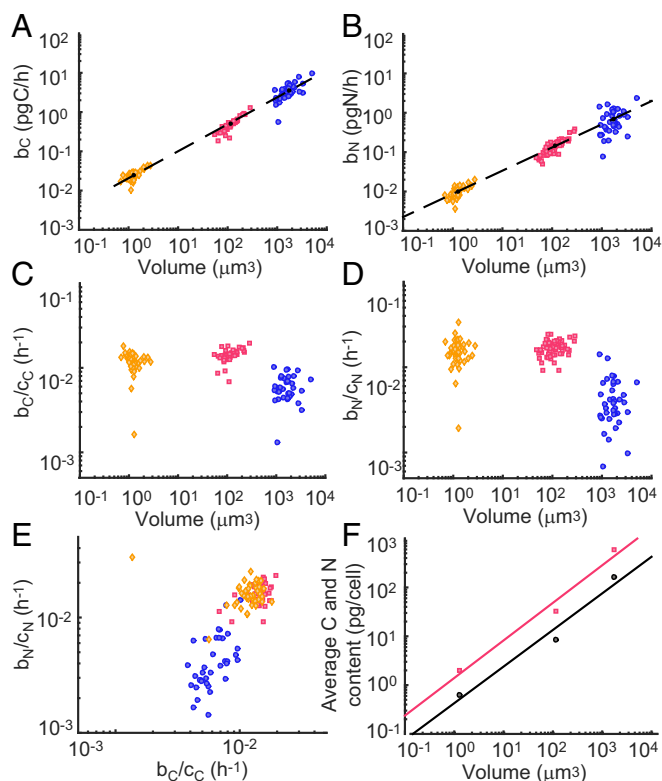


Fig. 2. (A and B) Plot of the single-cell uptake rate of (A) carbon and (B) nitrogen vs. single-cell volume for the 3 strains studied here. Black circles are species averages (V , b_C) and (V , b_N), while black dashed lines are linear least-squares fits of $(\log V, \log b_C)$ and $(\log V, \log b_N)$. Orange diamonds, *Synechococcus* sp.; pink squares, *S. obliquus*; blue circles, *C. ovata*. (C and D) Scatter plot of single-cell, carbon-specific carbon uptake rate (C) and nitrogen-specific nitrogen uptake rate (D) vs. single-cell volume for the 3 strains. (E) Scatter plot of single-cell, carbon-specific carbon uptake rates b_C/c_C (i.e., the carbon uptake rate b_C divided by the cell total carbon content c_C) and single-cell, nitrogen-specific nitrogen uptake rates b_N/c_N (i.e., the nitrogen uptake rate b_N divided by the cell total nitrogen content c_N). (F) Scaling of the average per-cell carbon (red squares) and nitrogen content (black circles) with average cell volume V , for the 3 phytoplankton strains. Lines are linear least-squares fits of log-transformed values.

scaling form in Eq. 2 could make the statistical test fail, although it would have little effect on the consequences of Eq. 2. In biological or ecological contexts, logarithmic corrections may be more important than in classical statistical physics, given that the sizes of the systems under investigation here are much farther from the thermodynamic limit than, say, a gas of $N \sim 10^{23}$ molecules. Finally, we estimated that the intraspecific volume heterogeneity explains only 34% to 58% of the observed variance of carbon uptake rates within one species and only 14% to 31% of the variance of nitrogen uptake rates (SI Appendix). Intrinsic variability, as given for example by phenotypic heterogeneity, is therefore a crucial contributor to the manifestation of biological variability and should be accounted for in any generalized scaling theory.

Discussion

When confronting the diversity of phytoplankton form and function, 2 broadly divergent approaches exist: one emphasizing the existence of master traits, such as cell size, that underlie much of the diversity, and the other emphasizing the importance of phylogenetic variability. The latter implies that taxonomic differences would be crucial to explain functional differences. Phytoplankton species are particularly relevant for the general study of size-dependent vital rates. On the one hand, in fact, changes in

phytoplankton community structure as a consequence of global changes in ocean chemistry and circulation, and in light and nutrient regimes, are expected to have major cascading effects on primary production, food web dynamics, the structure of the marine food web, and biogeochemical cycles (37). On the other hand, cell size has been shown to be a key determinant of phytoplankton metabolism and community structure (17, 38–41).

Our main result is that species that differ widely in their phylogenetic affiliation show patterns of intraspecific variability of metabolic rates and cell sizes that are identical, when appropriately rescaled according to the average species' mean cell size, as suggested by the collapses shown in Fig. 4 B and D. As a consequence, size predicts not only the average metabolic rate, as per Kleiber's law, but also the variability that is expected around that average. The scaling in Eq. 2 suggested by our results implies that such variability scales with a power of size, supporting size as a fundamental trait to determine the structure of microbial communities (17), and consequently their functioning and response to environmental fluctuations (22).

Eq. 2 predicts that the maximum and the minimum metabolic rates b_{\min} and b_{\max} that would be observed in a population of N individuals of the same species with average body size V scale with the same exponent as the average metabolic rate B ; i.e., $B \propto b_{\min} \propto b_{\max} \propto V^\alpha$ (SI Appendix). This suggests that discrepancies in the measured value of the scaling exponent α in the literature might not be explained merely by discrepancies of measurements (say, targeting basal, field, or maximum metabolic rates), but rather represent real shifts in the scaling exponents.

In this work, we characterized physiological variations of body size and metabolic rate within clonal populations at a constant temperature. In natural populations, different sources of variability will also be important, most notably genetic and environmental ones. An environmental variable that is well known to affect metabolic rate (42) and body size is temperature (31, 43), which enters the classical Kleiber's law through an Arrhenius-like term as $B \propto V^\alpha e^{-E/(kT)}$, where E is an activation energy, k is Boltzmann's constant, and T is the temperature. The most parsimonious way to account for the dependence of metabolic rates on temperature in the marginal distribution of metabolic rates would be to assume the following dependence of $p(b|V, T)$ on V and T : $p(b|V, T) = b^{-1} G \left[b / \left(V^\alpha e^{-E/(kT)} \right) \right]$. Experiments performed at different values of T are required to verify this hypothesis.

The limited number of cells that can be analyzed with the experimental approach adopted here precludes a detailed identification of the joint probability distribution of mass and metabolic rate, $p(v, b|V)$ (Materials and Methods), or the

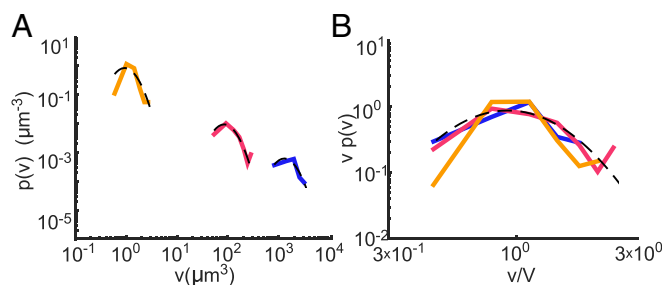


Fig. 3. (A) Experimental body size distributions $p(v|V)$ for the 3 freshwater species. Dashed lines are log-normal fits as predicted by ref. 31. (B) Collapse of the 3 distributions in A when plotted by rescaling $v p(v|V)$ vs. v/V . The dashed line in B is a quadratic least-squares fit of the average of the 3 collapsed curves and corresponds to a log-normal functional form for the nonrescaled curves (A). Orange, *Synechococcus* sp.; pink, *S. obliquus*; blue, *C. ovata*.

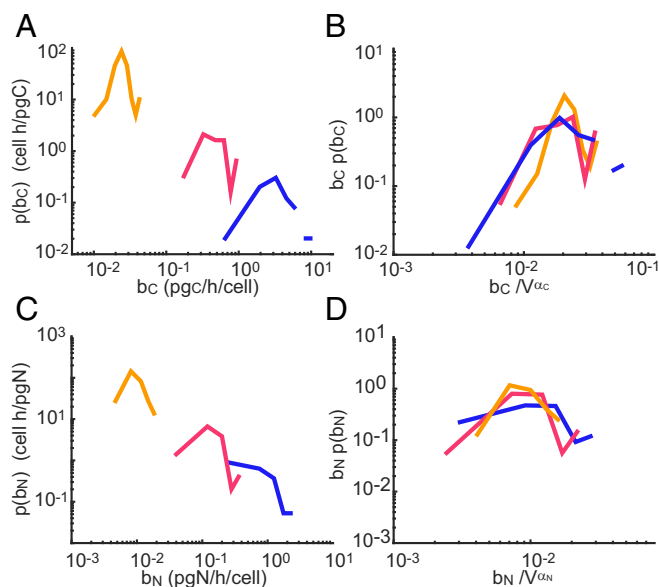


Fig. 4. (A) Intraspecific carbon uptake rate distributions $p(b_C|V)$ for the 3 strains. (B) Collapse of the 3 distributions in A obtained by plotting $b_C p(b_C|V)$ vs. b_C/V^{α_C} in a double-logarithmic plot (Materials and Methods). (C) Intraspecific nitrogen uptake rate distributions $p(b_N|V)$ for the 3 strains. (D) Collapse of the 3 distributions in C obtained by plotting $b_N p(b_N|V)$ vs. b_N/V^{α_N} in a double-logarithmic plot. Orange, *Synechococcus* sp.; pink, *S. obliquus*; blue, *C. ovata*.

identification of the effects of cell cycle stage or nutrient limitations (44). Because we posit that v and b are correlated random variables, their joint probability distribution cannot simply be obtained by the product of marginal; i.e., $p(v, b|V) \neq p(v|V) p(b|V)$. To study the full joint distribution, one must instead bin the experimental data both in body size and in metabolic rate, which requires a much greater number of analyzed cells for each species than that achievable with the experimental methods used here. Nevertheless, our measurements of the marginal distributions $p(v|V)$ and $p(b|V)$ constrain the possible form of the joint probability distribution $p(v, b|V)$ through the relationships $p(v|V) = \int p(v, b|V) db$ and $p(b|V) = \int p(v, b|V) dv$, where integration is carried out over the experimental ranges. The implications of our findings on the possible dependence of $p(v, b|V)$ on v , b and V given the constraints imposed by our measurements are briefly discussed in Materials and Methods.

Experimental circumstances may have limited the generality of our results, but nonetheless support the need for broader investigations along these lines. First, cultures were grown at likely subsaturating irradiance, which may have affected the observed size-scaling exponents (0.69 for carbon and 0.59 for nitrogen), which were lower than the exponents estimated in previous studies (in the range 0.8 to 0.9) obtained by measuring bulk rates of nutrient uptake under light-saturating conditions (7, 15, 35). Low light is known to induce a shallower slope in the scaling between metabolic rate and cell size, possibly because larger cells suffer from “package” effects (a reduction in chlorophyll-specific light absorption) that become progressively more important as light levels decrease (low light induces higher pigment content and therefore a lower absorption efficiency) (15). Second, determining the carbon and nitrogen content at the single-cell level would be a challenging major advance. In fact, our results rest on the assumption that individual elemental content can be predicted by cell volume by Eq. 4, although their relationship at the intraspecific level has not been tested to date. Combining electron-probe X-ray microanalysis (XRMA) for measurement of single-cell ele-

mental content with NanoSIMS analyses is a possible solution (45). Relatedly, experimental observations (16) have shown that, at the interspecific level, elemental content is a better predictor of metabolic rates than cell volume in phytoplankton, possibly because it is a better proxy for body mass. Therefore, relating metabolic rate to elemental content rather than volume would be a promising development.

Kleiber’s law is particularly valuable for its use in theoretical and computational models of community dynamics, because it allows theoretical ecologists to account for the dependence of metabolic rates of different species on their typical body size (16, 17, 46) via a simple power-law relationship that bypasses the need to explicitly account for each species’ physiology (4). This dependence has been used, for example, to predict the height distribution of trees in tropical forests (47), to explore the covariation of macroecological scaling laws (4), and to study the fluctuations of the number of species inhabiting islands of different areas (48). In all these applications, Kleiber’s law provides the link between the resources available in a given ecosystem and the consumption rate of individuals. Our characterization of the scaling of intraspecific variability of metabolic rates with body size is a first step toward understanding the intraspecific correlation of metabolic rate with body size and being able to account for intraspecific variability in theoretical and computational models of community dynamics. An outstanding question in this field is whether and how the correlated fluctuations of body size and metabolic rates at the individual level affect size-related ecological patterns such as the interspecific body size distribution and the species–area relationship at the community level. To get there, we first need to close the circle and identify how the joint distribution depends on v , b , and V .

In conclusion, common scaling features of body sizes and uptake rates are shown to hold for species of freshwater phytoplankton across 3 orders of magnitude in cell volume. Such features imply the collapse of distinct experimental distributions of body size and uptake rates onto a universal master curve once suitably rescaled. The foundations are thus provided for a unified framework for metabolic rate–organismic body size relations embedding fluctuations and operating across taxa and scales.

Materials and Methods

Labeling Experiment. Monocultures of the cyanobacterium *Synechococcus* sp., the chlorophyte *S. obliquus*, and the cryptophyte *C. ovata* obtained from the Culture Collection of Algae and Protozoa (CCAP) were grown in culture medium for freshwater diatoms (WC medium) at 20 °C under cool white light with a photon flux of 25 to 50 $\mu\text{E m}^{-2}\text{s}^{-1}$ and a 14 h light: 10 h darkness photoperiod. Samples were obtained during the exponential growth phase (17). Samples were incubated for 3 h in WC medium enriched in ^{13}C and ^{15}N (see SI Appendix for details) and then fixed in 1% paraformaldehyde. A comparison of cell volumes between fixed and unfixed cultures showed that fixation did not cause cell shrinkage.

NanoSIMS Measurements. NanoSIMS is an ion microprobe that performs mass spectrometry on secondary ions sputtered from the top few atomic monolayers of a solid target by the impact of a primary beam of charged particles (49). The high spatial resolution of the ion beam (~ 100 nm) allows the creation of an ion image of the sample through a raster of the primary beam on the sample surface. The color of a pixel of the ion image corresponds to the counts of that ion obtained from the sputtering of that pixel. The ratios $r_C = {}^{13}\text{C}/{}^{12}\text{C}$ and $r_N = {}^{15}\text{N}/{}^{14}\text{N}$ in each pixel can be obtained from a ratio of the appropriate ion images (27). For each species, we prepared a control sample before incubation and an enriched sample after incubation for NanoSIMS analysis by filtering fixed culture on polycarbonate filters (23, 27) (SI Appendix). Cells were bombarded with a beam of Cs^+ ions focused to a spot of about 180 nm on the sample surface. Secondary ion images for ${}^{12}\text{C}^{14}\text{N}^-$, ${}^{12}\text{C}^{15}\text{N}^-$, ${}^{12}\text{C}_2^-$, and ${}^{13}\text{C}^{12}\text{C}^-$ were simultaneously recorded. We obtained ratio images from the ratio of the ${}^{12}\text{C}^{15}\text{N}^-$ and ${}^{12}\text{C}^{14}\text{N}^-$ images and of the ${}^{13}\text{C}^{12}\text{C}^-$ and ${}^{12}\text{C}_2^-$ images (see Fig. 1 for examples). Details of the instrument settings, of the procedures, and on the conversion of the measured ratios to ${}^{13}\text{C}:{}^{12}\text{C}$ and ${}^{15}\text{N}:{}^{14}\text{N}$ ratios can be found in SI Appendix. The average C and N content of cells, necessary to compute the total C and N

uptake during the incubation period, was measured by gas chromatography (SI Appendix).

Computation of Size and Uptake Rates. Regions of interest (ROIs) were defined for each imaged cell, following its contour (Fig. 1). A total of, respectively, 37, 54, and 35 cells were imaged for each species. Individual cell volumes were inferred from cell cross-sections by measuring the axes and assuming a spherical cell shape for *Synechococcus* and an ellipsoidal one for *Scenedesmus* and *Cryptomonas*, as in ref. 50. Average isotope ratios r_C and r_N of each single cell were obtained by averaging the values of all of the ROI pixels in the corresponding ratio image. In doing so, we assumed that the analyzed layer was representative of the entire cell. For each imaged cell, the uptake rate b_i of each cell, where $i = C, N$, was computed by the relation

$$b_i = \frac{(\bar{r}_i - \bar{r}_{i,0})c_i}{\bar{r}_{i,med}} \frac{1}{\Delta t}, \quad [3]$$

where $\bar{r}_i = r_i/(1 + r_i)$ are, respectively, the ratios $^{13}\text{C}:\text{C}$ and $^{15}\text{N}:\text{N}$; $\bar{r}_{i,0}$ are the natural ratios $^{13}\text{C}:\text{C}$ and $^{15}\text{N}:\text{N}$ measured in the control sample; $\bar{r}_{i,med}$ are the $^{13}\text{C}:\text{C}$ and $^{15}\text{N}:\text{N}$ ratios in the incubation medium; Δt is the incubation time; and c_i is the total cell content of, respectively, C and N. The values of c_i are computed from the average carbon and nitrogen content measured for each species, C_C and C_N , assuming that they scale sublinearly with the average cell volume of that species V ; i.e., $C_i \propto V^{\gamma_i}$ with $\gamma_i < 1$, where $i = C, N$. A sublinear scaling of the carbon content with the average cell volume V has been observed in several studies (51), with γ_C ranging from 0.76 to 1.04 in measurements from tens of taxa covering several orders of magnitude in cell volume. From our measurements on the 3 species covering 3 orders of magnitude in cell volume, we found $\gamma_C = 0.8 \pm 0.1$ and $\gamma_N = 0.8 \pm 0.1$ (mean \pm SD; Fig. 2F). By assuming that the scaling holds at the individual cell level within a species, c_i is obtained as

$$c_i = k_i \langle c_i \rangle \left(\frac{V}{V} \right)^{\gamma_i}, \quad [4]$$

where $k_i \simeq 1$ is a constant independent of individual or species identity (SI Appendix).

Scaling Functional Form of $p(v|V)$. We find that the function F from Eq. 1 obtained from the data collapse of Fig. 3B is fitted well by a parabola in log-log space ($R^2 = 0.86$), corresponding to a log-normal distribution of body sizes (31) derived from a normal distribution with variance σ and mean $\mu = -\sigma^2/2$. The parameter $\sigma = 0.46$ (95% confidence interval [0.38, 0.53]) was estimated by fitting a parabola to the average of the 3 rescaled volume distributions (Fig. 3B). Note that this is a 1-parameter fit because a log-normal distribution has the scaling form of Eq. 1 only if $\mu = -\sigma^2/2$. The resulting log-normal fits of the size distribution are shown in Fig. 3A. Note that even though $p(v|V)$ is well fitted by a log-normal distribution, the identification of the exact form of F is not necessary for verifying Eq. 1.

Elements for a Further Generalization of Kleiber's Law. Experimental results allowed the characterization of the marginal distribution of metabolic rates (2). b and v being 2 correlated variables, their joint distribution is not simply given by the product of the 2 marginals, but rather by $p(v, b|V) = p(v|V)p(b|v, V)$, where $p(b|v, V)$ is the distribution of metabolic rates conditional on both the species typical body size V and the body size v of the individual. The scaling properties of $p(b|v, V)$ cannot be inferred from the available experimental data since they would require binning in both v and b and very few data would fall in each bin. Nevertheless, knowing that $p(b|v, V)$ must be compatible with the form of the marginal $p(b|V)$, we can make reasonable hypotheses on its shape. In particular, we can distinguish 2 cases, depending on whether the intraspecific size scaling of b has the same exponent α as the interspecific scaling, or a different one. The 2 cases are both compatible with the form of $p(b|V)$ supported by the data (Eq. 2), but the data do not allow distinguishing between the 2 for 2 reasons. First, the number of data points is not sufficient to verify the scaling form of $p(b|v, V)$. Second, the intraspecific scaling of b shown in Fig. 2 A and B is affected by

our assumption that the C and N content of cells scales with volume at the intraspecific level with the same exponent of the interspecific scaling. This assumption needs to be verified experimentally before drawing conclusions regarding the intraspecific scaling of metabolic rates $\langle b|v, V \rangle$ with v . The 2 cases are as follows:

Case 1. In the case in which the intraspecific scaling of b has the same exponent of the interspecific scaling, a reasonable further assumption is

$$p(b|v, V) = p(b|v) = \frac{1}{b} \tilde{G}_1 \left(\frac{b}{v^\alpha} \right), \quad [5]$$

where \tilde{G}_1 is a function with the same properties of G (SI Appendix). Note that Eq. 5 (but not our Eq. 2, in which $p(b|V)$ is conditional on the average species' mass) corresponds to equation 2 of ref. 14, where data on the metabolic rate of small mammals were shown to be compatible with it (to show that Eq. 5 and equation 2 of ref. 14 coincide, one needs to multiply and divide Eq. 5 by v^α and recognize that $(b/v^\alpha)^{-1} \tilde{G}_1(b/v^\alpha)$ is still a function of b/v^α). This assumption means that, knowing the individual body size v , the average species body size V does not give any further information on the individual metabolic rate. This hypothesis implies that $\langle b|v, V \rangle = \int db b p(b|v, V) \propto v^\alpha$ (SI Appendix); therefore α is the exponent of the intraspecific size scaling of b . The joint distribution would then have the form

$$p(v, b|V) = \frac{1}{vb} F \left(\frac{v}{V} \right) \tilde{G}_1 \left(\frac{b}{v^\alpha} \right) = \frac{1}{vb} H_1 \left(\frac{v}{V}, \frac{b}{v^\alpha} \right), \quad [6]$$

where $H_1(x, y) = F(x) \tilde{G}_1(y/x^\alpha)$. This form for the joint probability distribution is compatible with the marginal distribution in Eq. 2, for which $\langle b|V \rangle \propto V^\alpha$; i.e., the exponent of the interspecific scaling of $\langle b|V \rangle$ with V is equal to α .

Case 2. If the intraspecific scaling of b has a different scaling exponent than the interspecific one, we can hypothesize

$$p(b|v, V) = \frac{1}{b} \tilde{G}_2 \left(\frac{b}{v^\alpha}, \frac{v}{V} \right). \quad [7]$$

See SI Appendix for the properties of $\tilde{G}_2(x, y)$. Eq. 7 implies

$$\langle b|v, V \rangle = \int_0^\infty b p(b|v, V) db = v^\alpha Q \left(\frac{v}{V} \right), \quad [8]$$

where $Q(y) = \int_0^\infty \tilde{G}_2(x, y) dx$. To have a power-law intraspecific size scaling of b , we need therefore to ask $Q(y) \propto y^\eta$, which gives

$$\langle b|v, V \rangle \propto v^{\alpha+\eta} V^{-\eta}. \quad [9]$$

Therefore, intraspecifically (i.e., for fixed V) the scaling exponent is $\alpha + \eta$. In this case, the joint distribution has the form

$$p(v, b|V) = \frac{1}{vb} F \left(\frac{v}{V} \right) \tilde{G}_2 \left(\frac{b}{v^\alpha}, \frac{v}{V} \right) = \frac{1}{vb} H_2 \left(\frac{v}{V}, \frac{b}{v^\alpha} \right), \quad [10]$$

where $H_2(x, y) = F(x) \tilde{G}_2(y, x)$. This functional form for $p(v, b|V)$ is again compatible with the function form of Eq. 2 for the marginal distribution $p(b|V)$, and thus the interspecific scaling of $\langle b|V \rangle$ with V is equal to α .

ACKNOWLEDGMENTS. Funds from the Swiss National Science Foundation, through Projects 200021.157174, SINERGIA 2019 CRSII5.186422/1, and IZSEZ0.177302 are gratefully acknowledged. A.G. thanks the Swiss National Science Foundation for funding through projects P2ELP2.168498 and P400PB.180823. This work was partly supported by a grant from the Simons Foundation (542395, to R.S.), as part of the Principles of Microbial Ecosystems Collaborative. A. Maritan thanks the Cariparo 2018 Excellence Projects for funding. We thank Frank Schreiber for suggestions on sample preparation and Aline Reynaud and Marta Reyes for precious help in the execution of the experiments.

1. M. Kleiber, Body size and metabolism. *Hilgardia* **6**, 315–353 (1932).
2. P. A. Marquet et al., Scaling and power-laws in ecological systems. *J. Exp. Biol.* **208**, 1749–1769 (2005).
3. I. A. Hattin et al., The predator-prey power law: Biomass scaling across terrestrial and aquatic biomes. *Science* **349**, aac6284 (2015).
4. S. Zaoli, A. Giometto, A. Maritan, A. Rinaldo, Covariations in ecological scaling laws fostered by community dynamics. *Proc. Natl. Acad. Sci. U.S.A.* **114**, 10672–10677 (2017).

5. J. H. Brown, J. F. Gillooly, A. P. Allen, V. M. Savage, G. B. West, Toward a metabolic theory of ecology. *Ecology* **85**, 1771–1789 (2004).
6. A. Ahluwalia, Allometric scaling in-vitro. *Sci. Rep.* **7**, 42113 (2012).
7. B. A. Ward, E. Marañón, B. Sauterey, J. Raut, D. Claessen, The size dependence of phytoplankton growth rates: A trade-off between nutrient uptake and metabolism. *Am. Nat.* **189**, 179–183 (2018).
8. P. McMahon, J. T. Bonner, *On Size and Life* (Scientific American, 1983).

9. R. H. Peters, *The Ecological Implications of Body Size* (Cambridge University Press, 1986).
10. V. M. Savage et al., The predominance of quarter-power scaling in biology. *Funct. Ecol.* **18**, 257–282 (2004).
11. G. B. West, J. H. Brown, B. J. Enquist, A general model for the origin of allometric scaling laws in biology. *Science* **276**, 122–126 (1997).
12. J. R. Banavar, A. Maritan, A. Rinaldo, Size and form in efficient transportation networks. *Nature* **399**, 130–132 (1999).
13. J. H. Brown, *Macroecology* (University of Chicago Press, Chicago, IL, 1995).
14. P. S. Dodds, D. H. Rothman, J. S. Weitz, Re-examination of the '3/4'-law of metabolism. *J. Theor. Biol.* **209**, 9–27 (2001).
15. D. S. Glazier, Beyond the 3/4: Variation in the intra- and interspecific scaling of metabolic rate in animals. *Biol. Rev. Camb. Philos. Soc.* **80**, 611–632 (2005).
16. E. Marañón et al., Unimodal size scaling of phytoplankton growth and the size dependence of nutrient uptake and use. *Ecol. Lett.* **16**, 371–379 (2013).
17. E. Marañón, Cell size as a key determinant of phytoplankton metabolism and community structure. *Ann. Rev. Mar. Sci.* **7**, 241–264 (2015).
18. D. S. Glazier, Is metabolic rate a universal 'pacemaker' for biological processes? *Biol. Rev. Camb. Philos. Soc.* **90**, 377–407 (2015).
19. T. Kolokotronis, D. E. J. Van Savage, W. Fontana, Curvature in metabolic scaling. *Nature* **464**, 753–756 (2010).
20. J. R. Banavar, T. J. Cooke, A. Rinaldo, A. Maritan, Form, function, and evolution of living organisms. *Proc. Natl. Acad. Sci. U.S.A.* **111**, 3332–3337 (2014).
21. C. A. Price et al., Testing the metabolic theory of ecology. *Ecol. Lett.* **15**, 1465–1474 (2012).
22. B. Enquist, Scaling from traits to ecosystems: Developing a general trait driver theory via integrating trait-based and metabolic scaling theories. *Adv. Ecol. Res.* **52**, 249–318 (2015).
23. F. Schreiber et al., Phenotypic heterogeneity driven by nutrient limitation promotes growth in fluctuating environments. *Nat. Microbiol.* **1**, 16055 (2016).
24. M. E. Malerba, M. M. Palacios, Y. M. Palacios Delgado, J. Beardall, D. J. Marshall, Cell size, photosynthesis and the package effect: An artificial selection approach. *New Phytol.* **219**, 449–461 (2018).
25. A. K. Pettersen, D. J. Marshall, C. R. White, Understanding variation in metabolic rate. *J. Exp. Biol.* **221**, jeb166876 (2018).
26. E. Kussell, S. Leibler, Phenotypic diversity, population growth, and information in fluctuating environments. *Science* **309**, 2075–2078 (2005).
27. M. Zimmermann et al., Phenotypic heterogeneity in metabolic traits among single cells of a rare bacterial species in its natural environment quantified with a combination of flow cell sorting and NanoSIMS. *Front. Microbiol.* **6**, 243–254 (2015).
28. N. Welkenhuysen et al., Single-cell study links metabolism with nutrient signaling and reveals sources of variability. *BMC Syst. Biol.* **11**, 59 (2017).
29. F. A. Labra, P. A. Marquet, F. Bozinovic, Scaling metabolic rate fluctuations. *Proc. Natl. Acad. Sci. U.S.A.* **104**, 10900–10903 (2007).
30. A. P. Allen, J. F. Gillooly, J. H. Brown, Linking the global carbon cycle to individual metabolism. *J. Exp. Biol.* **19**, 202–213 (2005).
31. A. Giometto, F. Altermatt, F. Carrara, A. Maritan, A. Rinaldo, Scaling body size fluctuations. *Proc. Natl. Acad. Sci. U.S.A.* **110**, 4646–4650 (2013).
32. T. Hama et al., Measurement of photosynthetic production of a marine phytoplankton population using a stable ^{13}C isotope. *Mar. Biol.* **73**, 31–36 (1983).
33. M. D. Johnson et al., Universal constant for heat production in protists. *Proc. Natl. Acad. Sci. U.S.A.* **106**, 6696–6699 (2009).
34. P. G. Falkowski, H. Lin, M. Y. Gurbunov, What limits photosynthetic energy conversion efficiency in nature? Lessons from the oceans. *Proc. Natl. Acad. Sci. U.S.A.* **106**, 6696–6699 (2017).
35. M. Olofsson et al., High single cell diversity in carbon and nitrogen assimilation by a chain-forming diatom across a century: Single cell diversity in *skeletonema*. *Environ. Microbiol.* **21**, 12941–12945 (2019).
36. S. M. Bhattacharjee, F. Seno, A measure of data collapse for scaling. *J. Phys. A Math. Gen.* **34**, 6375–6380 (2001).
37. Z. V. Finkel et al., Phytoplankton in a changing world: Cell size and elemental stoichiometry. *J. Plankton Res.* **32**, 119–137 (2009).
38. S. W. Chisholm, "Phytoplankton size" in *Primary Productivity and Biogeochemical Cycles in the Sea*, P. G. Falkowski, A. D. Woodhead, K. Vivirito, Eds. (Springer US, Boston, MA, 1992), pp. 213–237.
39. Z. V. Finkel, J. V. Irwin, Modeling size-dependent photosynthesis: Light absorption and the allometric rule. *J. Theor. Biol.* **204**, 361–369 (2000).
40. A. J. Irwin, Z. V. Finkel, O. M. P. Schofield, P. G. Falkowski, Scaling-up from nutrient physiology to the size-structure of phytoplankton communities. *J. Plankton Res.* **28**, 459–471 (2006).
41. T. Key et al., Cell size trade-offs govern light exploitation strategies in marine phytoplankton. *Environ. Microbiol.* **12**, 95–104 (2010).
42. J. F. Gillooly, J. H. Brown, G. B. West, V. M. Savage, E. L. Charnov, Effects of size and temperature on metabolic rate. *Science* **293**, 2248–2251 (2001).
43. M. Daufresne, K. Lengfellner, U. Sommer, Global warming benefits the small in aquatic ecosystems. *Proc. Natl. Acad. Sci. U.S.A.* **106**, 12788–12793 (2009).
44. K. Banse, Rates of growth, respiration and photosynthesis of unicellular algae as related to cell size. *J. Phycol.* **12**, 135–140 (1976).
45. M. Segura-Noguera, D. Blasco, J. M. Fortuño, An improved energy-dispersive X-ray microanalysis method for analyzing simultaneously carbon, nitrogen, oxygen, phosphorus, sulfur, and other cation and anion concentrations in single natural marine microplankton cells. *Limnol. Oceanogr. Methods* **10**, 666–680 (2012).
46. E. Marañón, P. Cermeño, M. Latasa, R. D. Tadonlèké, Temperature, resources, and phytoplankton size structure in the ocean. *Limnol. Oceanogr.* **57**, 1266–1278 (2012).
47. T. Anfodillo et al., An allometry-based approach for understanding forest structure, predicting tree-size distribution and assessing the degree of disturbance. *Proc. R. Soc. Lond. B Biol. Sci.* **280**, 2375 (2012).
48. S. Zaoli, A. Giometto, J. Giezendanner, A. Maritan, A. Rinaldo, On the probabilistic nature of the species-area relation. *J. Theor. Biol.* **462**, 391–407 (2019).
49. P. Hoppe, S. Cohen, A. Meibom, NanoSIMS: Technical aspects and applications in cosmochemistry and biological geochemistry. *Geostand. Geoanal. Res.* **37**, 111–154 (2013).
50. I. Olenina et al., "Biovolumes and size-classes of phytoplankton in the Baltic Sea" in *Helcom Baltic Sea Environment Proceedings No. 106* (Helsinki Commission, 2006), pp. 144.
51. V. Gosselain, P. B. Hamilton, J. P. Descy, Estimating phytoplankton carbon from microscopic counts: An application for riverine systems. *Hydrobiologia* **438**, 75–90 (2000).